HIPPOCAMPUS 26:1525–1541 (2016)

Gain Modulation of Cholinergic Neurons in the Medial Septum-Diagonal Band of Broca Through Hyperpolarization

Eric D. Melonakos,[1]* John A. White,[1,2] and Fernando R. Fernandez[1,2]

ABSTRACT: Hippocampal network oscillations are important for learning and memory. Theta rhythms are involved in attention, navigation, and memory encoding, whereas sharp wave-ripple complexes are involved in memory consolidation. Cholinergic neurons in the medial septum-diagonal band of Broca (MS-DB) influence both types of hippocampal oscillations, promoting theta rhythms and suppressing sharp wave-ripples. They also receive frequency-dependent hyperpolarizing feedback from hippocamposeptal connections, potentially affecting their role as neuromodulators in the septohippocampal circuit. However, little is known about how the integration properties of cholinergic MS-DB neurons change with hyperpolarization. By potentially altering firing behavior in cholinergic neurons, hyperpolarizing feedback from the hippocampal neurons may, in turn, change hippocampal network activity. To study changes in membrane integration properties in cholinergic neurons in response to hyperpolarizing inputs, we used whole-cell patch-clamp recordings targeting genetically labeled, choline acetyltransferase-positive neurons in mouse brain slices. Hyperpolarization of cholinergic MS-DB neurons resulted in a long-lasting decrease in spike firing rate and input-output gain. Additionally, voltage-clamp measures implicated a slowly inactivating, 4-AP-insensitive, outward K^+ conductance. Using a conductance-based model of cholinergic MS-DB neurons, we show that the ability of this conductance to modulate firing rate and gain depends on the expression of an experimentally verified shallow intrinsic spike frequency-voltage relationship. Together, these findings point to a means through which negative feedback from hippocampal neurons can influence the role of cholinergic MS-DB neurons. © 2016 Wiley Periodicals, Inc.

KEY WORDS: spike firing; voltage-gated K^+ conductance; exponential integrate-and-fire model; acetylcholine; electrophysiology

This article was published online on September 15, 2016. After online publication text corrections were made. This notice is included in the online and print versions to indicate that both have been corrected on September 24, 2016.

[1] **Department of Bioengineering, University of Utah, Salt Lake City, Utah;** [2] **Department of Biomedical Engineering, Boston University, Boston, Massachusetts**

Grant sponsor: NIH; Grant number: R01MH085074; Grant sponsor: NIH; Grant number: R03MH103728.

Abbreviations used: MS-DB, medial septum-diagonal band of Broca; SPW-R, sharp wave-ripple; *f-I* curve, frequency-current curve; $ChAT^+$, choline acetyltransferase-positive; *f-V* curve, frequency-voltage curve; ACSF, artificial cerebrospinal fluid; AHP, afterhyperpolarization; *I-V*, current-voltage; 4-AP, 4-aminopyridine; eLIF, exponential leaky integrate-and-fire; LIF, leaky integrate-and-fire; I_{siK}, slowly inactivating K^+ current; SD, standard deviation.

*Correspondence to: Eric D. Melonakos, Department of Bioengineering, University of Utah, 36 Wasatch Drive, Salt Lake City, UT 84112. E-mail: eric.melonakos@gmail.com

Accepted for publication 30 August 2016.
DOI 10.1002/hipo.22653
Published online 2 September 2016 in Wiley Online Library (wileyonlinelibrary.com).

INTRODUCTION

Hippocampal electrical oscillations are thought to be critical for information processing. For example, theta rhythms (4 − 12 Hz) are correlated with attention, navigation, and memory encoding (Berry and Thompson, 1978; Winson, 1978; see Buzsáki, 2005, for review; Hasselmo, 2005), whereas sharp wave-ripple complexes (SPW-Rs; 140 − 220 Hz) are important for memory consolidation (Girardeau et al., 2009). Both rhythms are influenced by the medial septum-diagonal band of Broca (MS-DB) (Winson, 1978; Vandecasteele et al., 2014), which contains GABAergic, cholinergic, and glutamatergic neurons and innervates the hippocampus via the fornix.

During theta rhythms, cholinergic MS-DB neurons are thought to tonically depolarize pyramidal and basket neurons in the hippocampus (Chapman and Lacaille, 1999), and are responsible for maintaining theta amplitude (Kramis et al., 1975; Lee et al., 1994; Gerashchenko et al., 2001; Zhang et al., 2011), while at the same time attenuating hippocampal SPW-Rs (Vandecasteele et al., 2014). During SPW-Rs, MS-DB neuron firing is suppressed (Dragoi et al., 1999). The source of this suppression is most likely feedback connections from the hippocampus (Alonso and Köhler, 1982) which provide inhibitory input to MS-DB neurons (Tóth et al., 1993; Jinno et al., 2007; Takács et al., 2008). This inhibitory feedback includes both fast GABAergic input from somatostatin-positive neurons (Jinno et al., 2007), primarily targeting GABAergic MS-DB neurons, and long-lasting hyperpolarizing feedback, primarily targeting cholinergic MS-DB neurons (Mattis et al., 2014). The long-lasting hyperpolarizing feedback is evoked most effectively following SPW-R frequency stimulation (as opposed to theta frequency stimulation) of hippocamposeptal neurons. This may point to a functional link between cholinergic neuron membrane voltage modulation and hippocampal network oscillation frequency. By altering firing behavior in cholinergic neurons, hyperpolarizing feedback from the hippocampus to cholinergic neurons may, in turn, change hippocampal network activity. However, little is known about the integration properties of cholinergic neurons in the MS-DB and how hyperpolarization affects the overall integration properties in these neurons.

Hyperpolarization of cholinergic neurons could deinactivate an "A-current", a K^+ current previously shown to be expressed in these neurons (Segal and Barker, 1984; Griffith and Sim, 1990; Markram and Segal, 1990). Furthermore, previous work has shown that recruitment of an A-current can decrease both the overall spike firing rate as well as the slope, or gain, of the frequency-current relationship (*f-I* curve) in neurons (Connor and Stevens, 1971; Heath et al., 2014; Patel and Burdakov, 2015). We hypothesized that hyperpolarization of MS-DB neurons may allow for activation of voltage-gated K^+ conductances consistent with an A-current and fundamentally alter the integration properties and spike output characteristics of cholinergic neurons.

Using whole-cell patch-clamp in mouse brain slices and targeting genetically labeled choline acetyltransferase-positive ($ChAT^+$) neurons, we show that hyperpolarization of cholinergic MS-DB neurons results in a long-lasting decrease in firing rate and gain. Additionally, our results indicate that a slowly inactivating, 4-AP-insensitive, outward K^+ conductance, distinct from the A-current, is responsible. Finally, we demonstrate that the modulation of firing rate and gain through hyperpolarization and recruitment of a K^+ current depends on the expression of a shallow spike frequency-voltage relationship (*f-V* curve). Together, these findings show that hyperpolarization alters the integrative properties of cholinergic MS-DB neurons, reducing their firing rate and gain, through the recruitment of a slowly inactivating K^+ conductance.

MATERIALS AND METHODS

All of the University of Utah Institutional Animal Care and Use Committee guidelines and provisions were followed.

Tissue Preparation

To create mice in which we could identify cholinergic neurons, we crossed ChAT-IRES-Cre knockin mice (B6;129S6-*Chat*$^{tm2(cre)Lowl}$/J, stock number 006410; Jackson Labs) with Ai9 mice possessing a loxP-flanked STOP cassette hindering transcription of tdTomato (B6;129S6-*Gt(ROSA)26Sor*$^{tm9(CAG\text{-}tdTomato)Hze}$/J, stock number 007905; Jackson Labs). From the resulting progeny of this crossing, we prepared coronal slices of the MS-DB from 54 mice (23 − 251 days old) of either sex. All chemicals were obtained from Sigma-Aldrich unless otherwise noted. Mice were anesthetized using isoflurane and decapitated, after which brains were removed and submersed in 0°C artificial cerebrospinal fluid (ACSF). Both slicing and recording ACSF solutions contained (in mM): 125 NaCl, 25 $NaHCO_3$, 25 D-glucose, 2.5 KCl, 2 $CaCl_2$, 1.25 NaH_2PO_4, and 1 $MgCl_2$, buffered to a pH of 7.4 using 95% O_2/5% CO_2. Immediately following submersion in ACSF, brains were sectioned using a vibratome (Leica VT1000 S; Leica Biosystems) into 400-μm slices. Following sectioning, slices were transferred to an incubation chamber at 30°C for 20 min, after which the incubation chamber was cooled to room temperature (20°C). At the time of experiments, slices were transferred to a perfusion chamber under a microscope (Axioscope 2+; Zeiss) equipped to excite and visualize tdTomato fluorescence (excitation: 554 nm; emission: 581 nm). Each slice contained numerous fluorescing neurons, from which healthy ones were selected for electrophysiological recordings. The perfusion chamber temperature during recordings was between 32 and 34°C.

Electrophysiology

Recording micropipettes were drawn on a micropipette puller (P-97; Sutter Instruments) and filled with intracellular fluid comprised of (in mM): 136 K-gluconate, 4 KCl, 10 HEPES, 7 diTrisPhCr, 4 Na_2ATP, 2 $MgCl_2$, 0.3 Tris-GTP, and 0.2 EGTA, buffered to a pH of 7.4 using KOH. Electrophysiological experiments were completed using a MultiClamp 700B amplifier (Molecular Devices), and data was acquired using the Real-Time eXperiment Interface (Lin et al., 2010) at a sample rate of 10 kHz. Typical pipette resistance was 3 − 5 MΩ, and typical series resistance was 15 − 60 MΩ. Although relatively high, the series resistance during voltage-clamp experiments was sufficient to measure the presence and approximate size and kinetics of the slowly inactivating current (measurements ranged from −3.3 to 6.3 nA). We also compensated for series resistance using the Rs Compensation tool available in the MultiClamp 700B software (Bandwidth = 1.02 kHz, Correction = 50 − 80%). The perfusion ACSF for most experiments contained 10 μM DNQX and 50 μM picrotoxin to eliminate voltage fluctuations arising from synaptic activity.

Simulations

We used Matlab (R2011a; MathWorks) for all model simulations, and each model was solved using the forward Euler method with a time step of 0.01 ms. The membrane voltage of the model was governed by the following equation:

$$C\frac{dV}{dt} = -g_L(V-E_L)+g_L\Delta_T\exp\left(\frac{V-V_{th}}{\Delta_T}\right) - g_{siK}\,bh(V-E_{siK})-I_w+I_e+I_{noise},$$

where C is the membrane capacitance (81.9 pF), V is the membrane voltage, g_L is the leak conductance (1.3 nS), E_L is the leak reversal (−85 mV), Δ_T is the spike slope factor (2 mV default), V_{th} is the threshold voltage (−59.5 mV), g_{siK} is the slowly inactivating, outward K^+ conductance (30.1 nS maximum), b is the K^+ conductance activation, h is the K^+ conductance inactivation, E_{siK} is the K^+ reversal potential (−93.1 mV), I_w is the spike-dependent adaptation current, I_e is the input current, and I_{noise} is the noise current.

Equations governing the various currents are as follows:

$$\frac{dI_w}{dt} = \frac{g_w(V-E_L)-I_w}{\tau_w}$$

(spike−dependent adaptation current;

g_w = 0.1 nS, τ_w = 125 ms, each spike adds 2.5 pA to I_w)

$$\frac{db}{dt}=\frac{b_\infty-b}{\tau_b}$$
$$\left(K^+\text{conductance activation};\ \tau_b=152.7\ \text{ms}\right)$$
$$\frac{dh}{dt}=\frac{h_\infty-h}{\tau_h}$$
$$\left(K^+\text{conductance inactivation};\ \tau_h=11100\ \text{ms}\right)$$
$$b_\infty=0.14+\frac{0.81}{1+\exp\left(\frac{-22.46-V}{8.08}\right)}$$
$$\left(K^+\text{conductance steady-state activation}\right)$$
$$h_\infty=0.08+\frac{0.88}{1+\exp\left(\frac{-60.23-V}{-5.69}\right)}$$
$$\left(K^+\text{conductance steady-state inactivation}\right)$$

Following a threshold crossing of 0 mV, voltage was reset to −65 mV. We also added a current noise term, I_{noise}, in order to account for small membrane voltage fluctuations seen in the absence of any synaptic input. I_{noise} was generated using white noise that is low-pass filtered [100 Hz cutoff frequency (f_{cut})]. Noise signals were first constructed in the frequency domain using the frequency amplitude [$A(f)$] equation $A(f)=\sqrt{\frac{1}{(2\pi f_{cut})^2+(2\pi f)^2}}$, and then converted into time series using Matlab's *ifft* function. The standard deviation of the simulated voltage with noise was 0.6 ± 0.0006 mV at -79.5 ± 0.0009 mV for $\Delta_T=2$ mV and 0.7 ± 0.0006 mV at -79.1 ± 0.001 mV for $\Delta_T=10$ mV. The membrane resistance was 190.5 ± 1.1 MΩ for $\Delta_T=2$ mV and 196.1 ± 1.1 MΩ for $\Delta_T=10$ mV.

Data Analysis

All values and error bars are reported as mean ± SEM. Statistical tests were performed using an α-level of $P=0.05$ unless otherwise noted. Data analyses were performed using custom and built-in functions in Matlab. Input resistances, membrane capacitances, and membrane time constants were all extracted in current-clamp mode from current steps that elicited a subthreshold voltage change of 5 − 10 mV. Resting voltage was the average membrane potential while the current was held at 0 pA for 2 s. Spike frequency was calculated by counting spikes and dividing by the current step duration. Gain was calculated by linear regression analysis using Matlab's *regstats* function in the statistical toolbox. For both experimental and modeling gains, lines were fitted to all currents from threshold (i.e., firing rate > 0 spikes/s) to the first current step with the maximum firing rate. In many of the cases following hyperpolarization, the linear fits of the *f-I* curves had a low R^2 value, owing to the narrow dynamic range and few spike frequency data points. In these cases, fit accuracy was visually confirmed. During some experiments, current-based artificial synaptic noise was added using an Ornstein-Uhlenbeck process, as described in Fernandez et al. (2011), with a mean current of 0 pA, time constant of 10 ms, and SD of 20 − 30 pA.

For firing rate vs. time analyses, firing rate was calculated using a 3 s binning window that moved forward in 0.3 s steps. The depth (amplitude) of the afterhyperpolarization (AHP) was measured as the difference between the voltage at the threshold of the spike (the time of the maximum second derivative of the spike) and the minimum voltage during the AHP of the spike. AHP duration was defined as the time between crossing the spike threshold voltage on the downstroke and when the voltage recovered to 40% of its value relative to threshold. In order to get accurate measurements of AHP depth, AHPs were only measured for spikes that occurred before the last 0.05 s of the current pulse. We first averaged AHP measurements within each current pulse and then binned the average AHP measurements from different current pulses by spike firing rate.

For voltage-clamp data, baseline currents were zeroed offline, and leak currents were subtracted either manually using a linear fit of the subthreshold current-voltage (*I-V*) curve (for reversal potential experiments) or automatically using the MultiClamp 700B software (for activation and inactivation curve experiments). To determine the reversal potential of the slowly inactivating current, we calculated the x-intercept of the tail current-voltage curve found by stepping to a range of voltages following activation of the conductance. Although the voltage range and step size varied between trials [e.g. (in mV) −50 to −100, −60 to −110, and −50 to −125 in 5 mV steps; −65 to −72.5, −65 to −100, −65 to −90, and −65 to −85 in 2.5 mV steps], the reversal potential for each trial was calculated individually.

In our analysis of the activation and inactivation curves, conductance was calculated using $g=I/(V-E)$, with the reversal $E=-93.1$ mV. Activation and inactivation curves were fit using the sigmoidal function $f(V)=a+b\Big/\left(1+\exp\left(\frac{V_{1/2}-V}{k}\right)\right)$, where $V_{1/2}$ is the midpoint of the sigmoid, k is the slope, b is the maximum of the curve minus the offset, and a is the offset of the curve. For *I-V* curves, we measured the average subthreshold or suprathreshold interspike voltage in response to current steps in current-clamp mode. Suprathreshold interspike voltages were measured during the time between the end of the spike AHP (as defined above) and the inflection point of the next spike. For these and the *f-V* curves, the first 250 ms of the pulse was excluded from the voltage average to allow voltage to reach a steady-state. In one case, the voltage during an interspike interval was not included in the analysis due to the interspike interval occurring during the last 0.05 s of its current pulse. Resistance curves were derived from *I-V* curves by using running linear regressions of the *I-V* curves, with lines fitted to 15 pA windows that moved forward in 5 pA steps. The slope of each linear regression was taken to be the resistance at the average voltage over the fitted points. Resistances were then binned into 10 mV voltage bins. Average membrane voltage for the *f-V* curves included spikes.

The drugs 4-aminopyridine (4-AP; Sigma-Aldrich), hongotoxin-1 (Alomone Labs), XE991 (Tocris Bioscience), and

tetraethylammonium (TEA; Sigma-Aldrich) were added to the ACSF at appropriate concentrations during the experiments as indicated below.

RESULTS

Hyperpolarization Reduces Firing Rate and Gain in Cholinergic MS-DB Neurons

To address how hyperpolarization alters the integration properties of cholinergic neurons, we used brain slices of the MS-DB and specifically targeted cholinergic neurons using transgenic mice with Cre-dependent expression of the red fluorescent protein variant tdTomato in $ChAT^+$ neurons (Fig. 1A). For comparisons, we also made electrophysiological measures from non-cholinergic (non-fluorescent) neurons, the majority of which were fast-spiking, and likely GABAergic (Sotty et al., 2003; Mattis et al., 2014).

Initial characterization indicated that input resistance, membrane capacitance, and membrane time constant values were not significantly different between cholinergic neurons and non-cholinergic neurons at -77.8 ± 0.0002 mV (cholinergic vs. non-cholinergic: 350.4 ± 30.4 MΩ vs. 347.7 ± 52.3 MΩ; 81.9 ± 5.7 pF vs. 66.7 ± 15.1 pF; and 26.9 ± 2.2 ms vs. 25.5 ± 10.9 ms, respectively) (Fig. 1B; $0.964 \geq P \geq 0.252$, two-tailed unpaired *t*-tests; $n = 30$ cholinergic neurons vs. 11 noncholinergic neurons). Resting voltage for most cholinergic neurons was above spike threshold (-45.6 ± 1.5 mV; $n = 13$). To assess the impact of hyperpolarization on cholinergic neuron spike firing output, we started by hyperpolarizing neurons and quantifying the effect on the subsequent spike firing rate. In current-clamp mode, we held neurons at depolarized potentials (-43.0 ± 1.8 mV). We then delivered current pulses of varying magnitudes (-55 to -300 pA) in order to transiently hyperpolarize membrane voltage to -72.5 ± 2.0 mV for 0.5 s. Upon release from hyperpolarization, we measured the firing rate during the subsequent 4.5 s. We repeated this protocol for 24 pulses and averaged the firing rates over the pulses. For control experiments, neurons were held at depolarized (i.e., non-hyperpolarized) voltages (-44.0 ± 1.7 mV) before measuring firing rate. In cholinergic neurons, we observed that brief, hyperpolarizing current pulses led to a significant reduction in mean firing rate, with a >40% reduction in firing rate when normalized to the average control firing rate (Figs. 1Cii and 1Ciii; 1.6 ± 0.4 spikes/s compared to control rates of 2.9 ± 0.4 spikes/s; $P = 0.006$ for raw rates and 0.004 for normalized rates, two-tailed paired *t*-tests; $n = 12$). In contrast, in noncholinergic MS-DB neurons, hyperpolarization to -71.8 ± 2.3 mV evoked a non-significant increase in firing rate over control (-51.8 ± 3.3 mV) (Figs. 1Dii and 1Diii; 2.4 ± 0.4 spikes/s compared to control rates of 2.1 ± 0.4 spikes/s; $P = 0.376$ for raw rates and 0.197 for normalized rates, two-tailed paired *t*-tests; $n = 13$ and 12, respectively).

Given that brief bouts of hyperpolarization reduced the firing rate in cholinergic neurons, we were also interested to know if hyperpolarization could modulate the overall scaling of the input-output relationship and provide a mechanism of gain control in these neurons. To quantify the gain, we used the slope of the *f-I* curve. We measured the *f-I* curves of cholinergic MS-DB neurons using 5 s currents over a 200 pA range, delivered in 10 pA steps. Each current pulse in the series followed either 1 s hyperpolarization (-81.5 ± 0.3 mV) or depolarization (-50.8 ± 0.6 mV). Spike rheobase did not change significantly following hyperpolarization (96.8 ± 8.4 pA following hyperpolarization vs. 95.5 ± 7.9 pA following depolarization; $P = 0.0546$, two-tailed paired *t*-test; $n = 31$). However, we found that current pulses following hyperpolarization not only led to a reduction in firing rate compared to those following depolarization, but also led to a 0.5 ± 0.1-fold divisive (reduction in gain) effect on the *f-I* curve, reducing the mean gain from 37.8 ± 4.5 spikes/nA·s following depolarization to 19.5 ± 4.6 spikes/nA·s following hyperpolarization (Fig. 2Aiii, inset; $P < 0.001$, two-tailed paired *t*-test; $n = 30$). Conversely, non-cholinergic MS-DB neurons exhibited no significant difference between hyperpolarized (-82.1 ± 0.3 mV) and depolarized (-49.9 ± 0.9 mV) conditions, with gains of 211.1 ± 60.2 spikes/nA·s and 262.8 ± 57.1 spikes/nA·s, respectively (Fig. 2Biii, inset; $P = 0.192$, two-tailed paired *t*-test; $n = 10$). Thus, hyperpolarization, or the membrane voltage history, selectively modulates both the mean and scaling of spike output in cholinergic neurons.

Synaptic inputs present *in vivo* cause large membrane voltage fluctuations (Paré et al., 1998; Anderson et al., 2000). Synaptic fluctuations, or synaptic noise, can cause changes in neuronal gain (Fernandez et al., 2011). In order to observe the size of the gain reduction during noisy, *in vivo*-like conditions, we added artificial synaptic noise using an Ornstein-Uhlenbeck process (see Methods). We found that the gain reduction persisted under noisy conditions, with gains of 30.2 ± 3.5 spikes/nA·s following hyperpolarization and 50.3 ± 7.2 spikes/nA·s following depolarization (Fig. 2Ciii, inset; $P = 0.0002$, two-tailed paired *t*-test; $n = 18$), suggesting that *in vivo* membrane voltage fluctuations do not preclude the effect.

Voltage Dependence, Time Dependence, and Recovery Time of Hyperpolarization-Induced Firing Rate Reduction

To better quantify the hyperpolarization-induced reduction in firing rate we observed and to assess the dependence of the effect on the duration and amplitude of cholinergic neuron hyperpolarization, we further characterized the phenomenon in three different ways: the (1) voltage dependence, (2) time dependence, and (3) recovery time of the effect.

As shown in Figure 3A, the reduction of firing rate was induced gradually and became significantly larger with increasing hyperpolarization (Fig. 3Aii; $P = 0.003$; one-way ANOVA between the mean firing rates for the first 3 s following each hyperpolarization level; $n = 2$ to 7 neurons). The largest decrease in firing rate occurred as the membrane voltage was hyperpolarized to voltages below -60 mV prior to eliciting spike discharge ($P < 0.001$ for

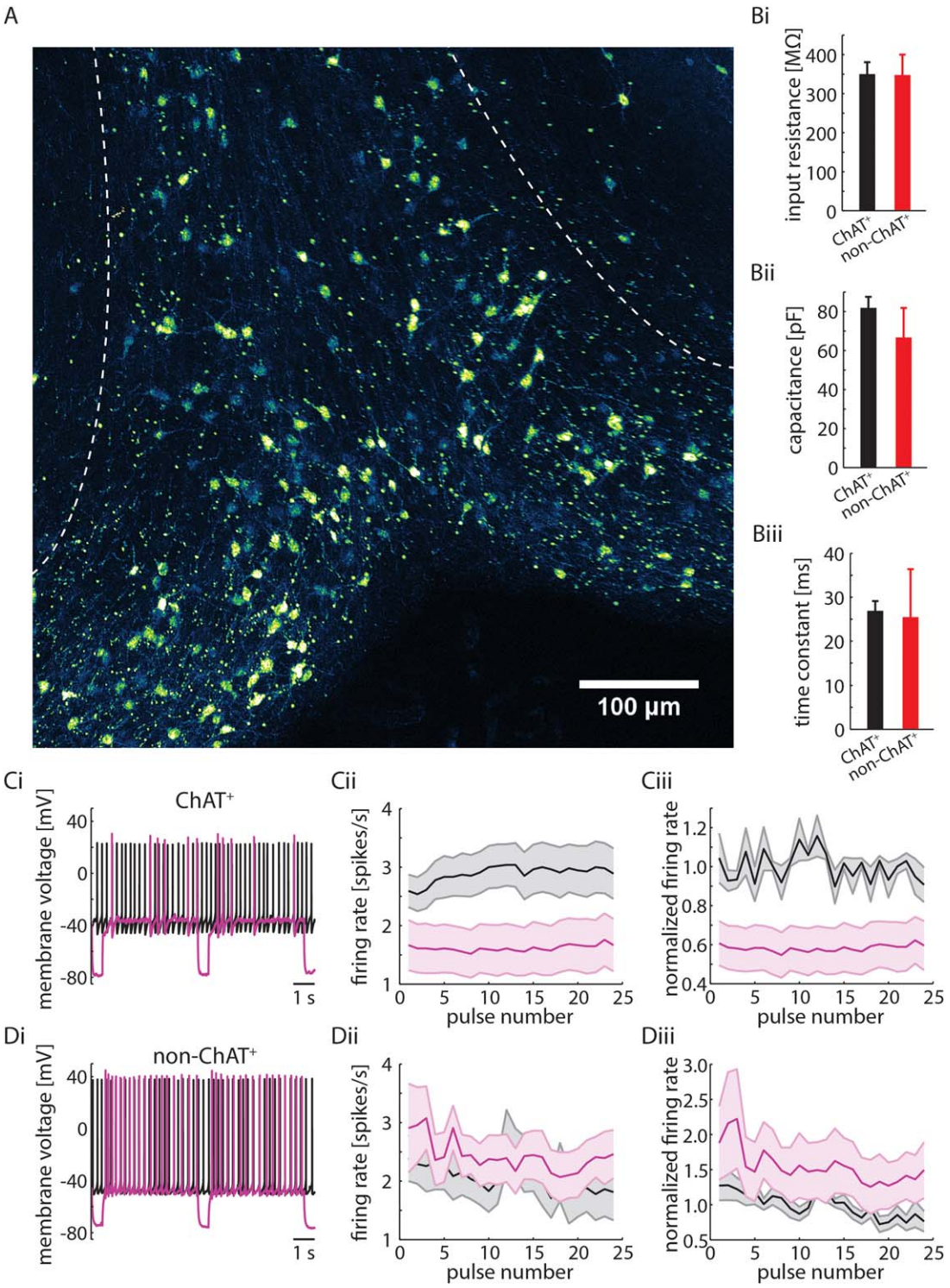

FIGURE 1. Hyperpolarization of cholinergic MS-DB neurons caused a reduction in firing rate. A: ChAT$^+$ neurons (green false color) in the MS-DB were identified using the transgenic expression of the fluorescent marker tdTomato. Dotted lines delineate approximate MS-DB boundaries. B: There were no significant differences between input resistance (*i*), membrane capacitance (*ii*), and membrane time constant (*iii*) values for ChAT$^+$ and non-ChAT$^+$ neurons. C: Brief hyperpolarization of ChAT$^+$ neurons to −72.5 mV resulted in a reduction in firing rate, as shown in an example (*i*), in averaged firing rates (*ii*), and in averaged normalized firing rates (*iii*). For C and D, data from hyperpolarizing pulses are shown in purple for visualization purposes. Throughout subsequent figures, gray lines indicate hyperpolarized data and black lines indicate depolarized data, unless otherwise specified. D: Hyperpolarization of non-ChAT$^+$ neurons to −71.8 mV did not result in a reduced firing rate and even led to non-significant increases in firing, as shown in an example (*i*), in averaged firing rates (*ii*), and in averaged normalized firing rates (*iii*). [Color figure can be viewed at wileyonlinelibrary.com]

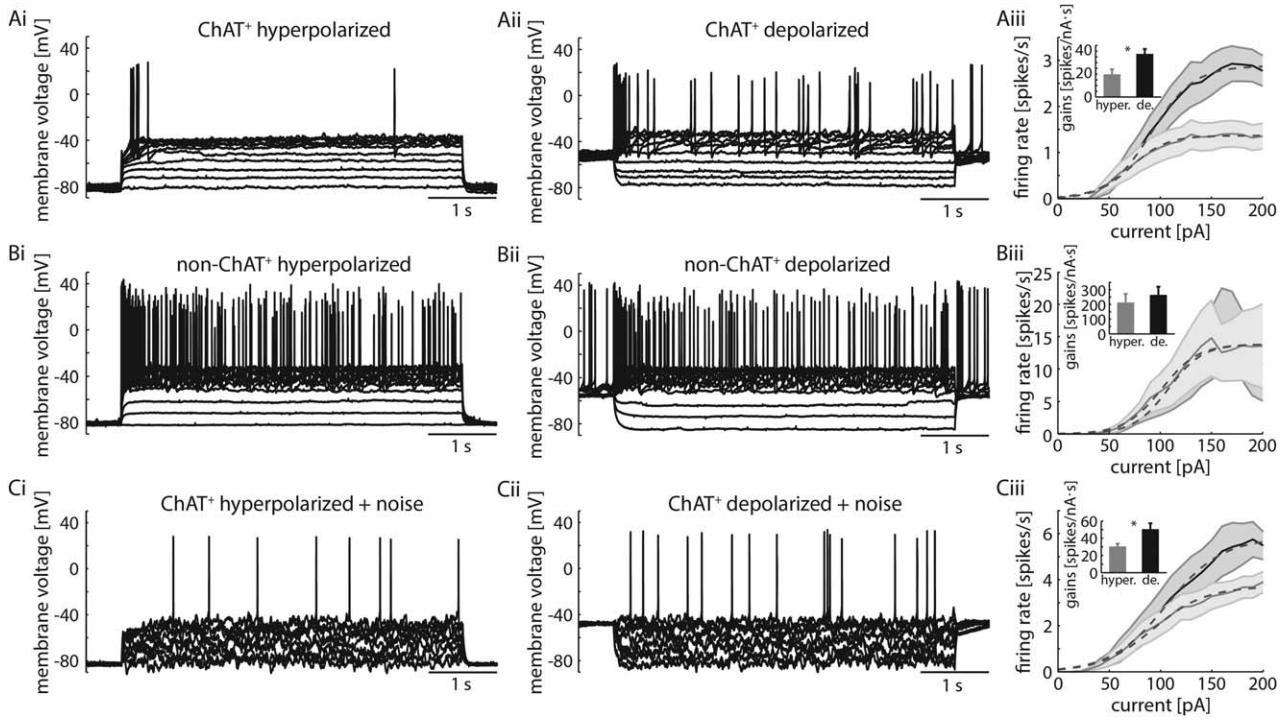

FIGURE 2. Hyperpolarization of cholinergic MS-DB neurons caused a divisive effect on the *f-I* curve. A: Hyperpolarization of a ChAT$^+$ neuron led to a divisive effect on the *f-I* curve. The sensitivity of the neuron to input currents following hyperpolarization (*i*) was less than that following depolarization (*ii*), as shown in the average *f-I* curve (*iii*). The average slope (gain) of the *f-I* curve is shown in A*iii*, *inset*. B: Hyperpolarization of non-ChAT$^+$ neurons had no significant effect on the *f-I* curve, as seen in examples *i* and *ii* and in the average *f-I* curve (*iii*). In these neurons, the gain (*iii*, *inset*) did not change in a voltage-history dependent manner. C: Hyperpolarization continued to significantly reduce gain in the presence of artificial synaptic noise (*iii*, *inset*). Sigmoidal fits of average *f-I* curves in A*iii*, B*iii*, and C*iii* (dashed lines) are for visualization purposes only.

comparison between hyperpolarization from −70 mV to −60 mV and hyperpolarization from −50 to −40 mV, $n = 6$ and 7, respectively; $P = 0.002$ for comparison between hyperpolarization from −70 mV to −60 mV and hyperpolarization from −40 mV and −30 mV, $n = 6$ and 2, respectively; $\alpha = 0.0083$, two-tailed unpaired *t*-tests). Likewise, greater durations in hyperpolarization increased the magnitude and time of the firing rate reduction (Fig. 3Bii; $P < 0.001$, one-way ANOVA between the mean firing rates for the first 3 s following each hyperpolarization time length; $n = 7$ neurons). Increasing hyperpolarization time from 0.05 s to 0.5 s (at -81.0 ± 1.1 mV) resulted in a significant decrease in firing rate ($P = 0.0006$; $\alpha = 0.0083$, two-tailed paired *t*-tests; $n = 7$ neurons). Further lengthening hyperpolarization time to 5 s did not result in a significant additional decrease in firing rate.

Next, we hyperpolarized neurons to -95.3 ± 3.9 mV for 10 s in order to quantify the amount of time it took cholinergic MS-DB neurons to recover to baseline firing rates after strong activation of the hyperpolarization-induced slowing of firing. We saw recovery to near-baseline rates after 60 s (Fig. 3Cii; $n = 7$). By fitting an exponential function to the firing rate following hyperpolarization, we found that recovery had an average time constant of 9.2 ± 3.3 s. Thus, hyperpolarization induces a reduction in subsequent firing rate that can last tens of seconds. Together, these findings show that cholinergic neurons, unlike other neurons in the MS-DB, reduce their firing rates for extremely long periods of time in response to relative short periods of hyperpolarization.

4-AP-Sensitive Currents Are Not Responsible for Hyperpolarization-Mediated Changes in Input-Output Properties

Fast-inactivating K^+ currents that activate and inactivate at subthreshold membrane voltages, known as "A-currents", lead to a delay to first spike (Segal and Barker, 1984) similar to that observed at the beginning of our traces from cholinergic neurons following hyperpolarization (e.g. in Fig. 2Ai). In addition, we observed a depolarizing notch in membrane voltage following hyperpolarization, which has also been observed in neurons that express an A-current (Connor and Stevens, 1971; Magariños-Ascone et al., 1999) (Fig. 4Bi, inset). Further, this current has been observed in other studies of cholinergic MS-DB neurons (Griffith and Sim, 1990; Markram and Segal, 1990). Because of its deinactivation with hyperpolarization, we hypothesized that an A-current could be responsible for the reduction in firing rate and gain through an increase in outward current following hyperpolarization.

To determine the involvement of an A-current in the gain reduction we observed, we bath applied 10 mM 4-aminopyridine (4-AP), a drug that blocks the K^+ channels that generate an A-current, among other currents. When 4-AP was added, the

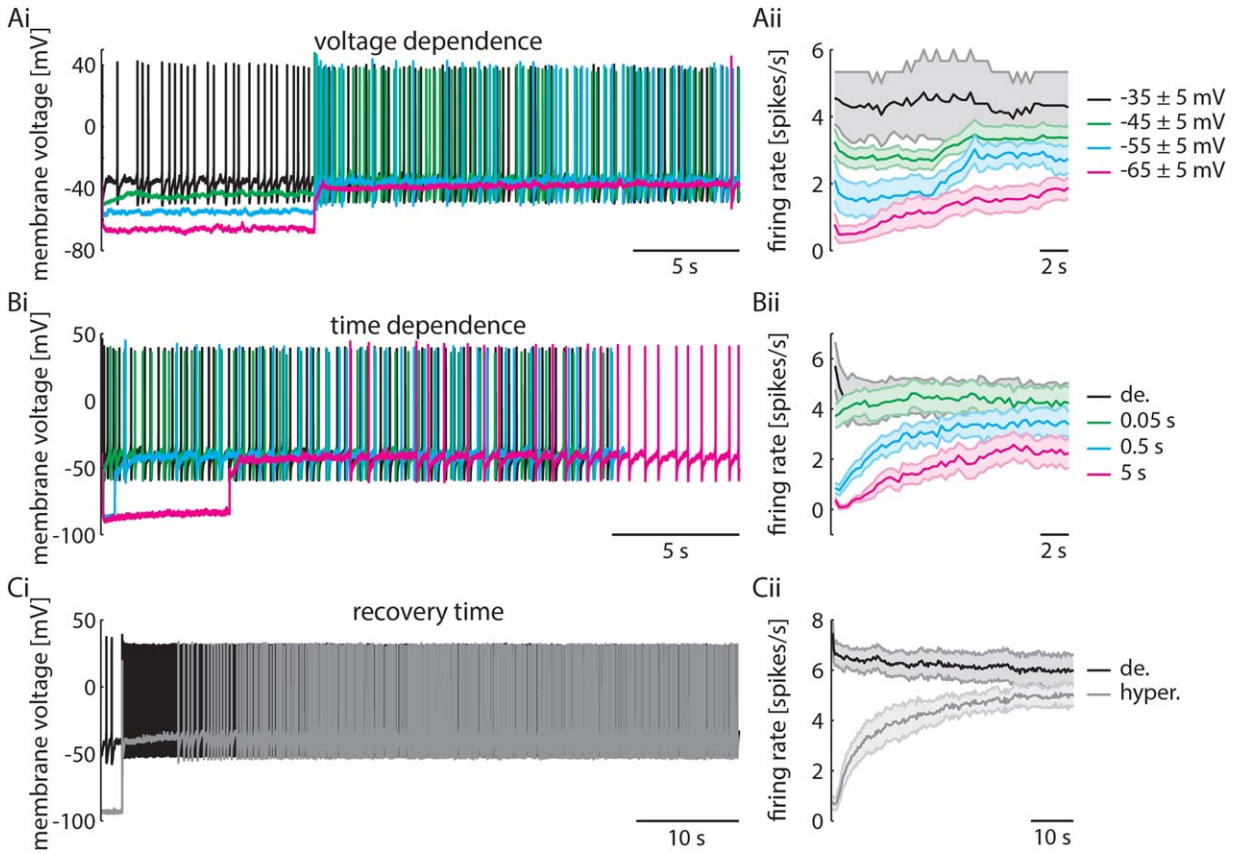

FIGURE 3. Characterization of the voltage dependence, time dependence, and recovery time of the hyperpolarization-induced firing rate reduction. A: Firing rate decreased during pulses following hyperpolarization as the level of hyperpolarization increased, as shown in example traces (*i*) and in averaged data (*ii*) for −30 to −40 mV ($n = 2$), −40 to −50 mV ($n = 7$), −50 to −60 mV ($n = 7$), and −60 to −70 mV ($n = 6$). B: Hyperpolarization to −81.0 mV for at least 0.5 s was necessary before firing rate reductions became significant, as shown in example traces (*i*) and averaged data (*ii*). Greater levels (A) and time lengths (B) of hyperpolarization led to progressively larger reductions in firing rate. C: Following strong activation of the effect, firing rates recovered to near-baseline values with a time constant of 9.2 s, as shown in example traces (*i*) and averaged data (*ii*). [Color figure can be viewed at wileyonlinelibrary.com]

characteristic notch in membrane voltage disappeared (Fig. 4Bii, inset) and the delay to first spike following hyperpolarization was reduced from an average of 450.3 ± 55.8 ms to 42.4 ± 7.0 ms (Figs. 4Bi and 4Bii; $P < 0.001$, two-way ANOVA; $n = 31$ neurons without 4-AP and 5 neurons with 4-AP). Despite the elimination of the delay and membrane voltage notch, the reduction in gain following hyperpolarization remained in the presence of 10 mM 4-AP, with gain decreasing from 44.1 ± 4.8 spikes/nA·s to 19.4 ± 8.0 spikes/nA·s following a 1 s long hyperpolarization to −81.2 ± 0.8 mV (Fig. 4C, inset; $P = 0.017$, two-tailed paired *t*-test; $n = 5$). Thus, although the A-current is responsible for the delay to first spike and the membrane notch following hyperpolarization, it is not responsible for the reduction in gain following hyperpolarization in cholinergic MS-DB neurons.

Cholinergic MS-DB Neurons Express a Slowly Activating and Inactivating, Voltage-Gated K^+ Current

Consistent with the lack of effect of 4-AP on firing rate and gain following hyperpolarization, A-currents typically inactivate with a time constant of less than 100 ms (Segal and Barker, 1984; Zona et al., 1988; Griffith and Sim, 1990; Bekkers, 2000), a time frame too short to account for the effects of hyperpolarization on cholinergic neurons. For this reason, we hypothesized that an outward K^+ current that is deinactivated by hyperpolarization, but with activation and inactivation kinetics much slower than a typical A-current, could be responsible for the changes in firing rate and gain. To determine the presence of this current, we performed voltage-clamp experiments with bath applied 10 mM 4-AP and 500 nM TTX. Note that we confirmed the presence of the A-current in voltage-clamp and eliminated it from our recordings with 4-AP (see Figs. 5Bi and 5Bii for sample recordings without and with 4-AP, respectively).

In voltage-clamp, we observed a large and slowly inactivating outward current in response to a depolarizing step to 0 mV from a holding voltage of −80 mV (Figs. 5Ai and 5Aii). To calculate the reversal potential of the current, we hyperpolarized to −80 mV for 30 s to deinactivate the channels, followed by depolarizing to −30 mV for 5 s, which was then followed by a step ranging from −50 to −125 mV (see Methods).

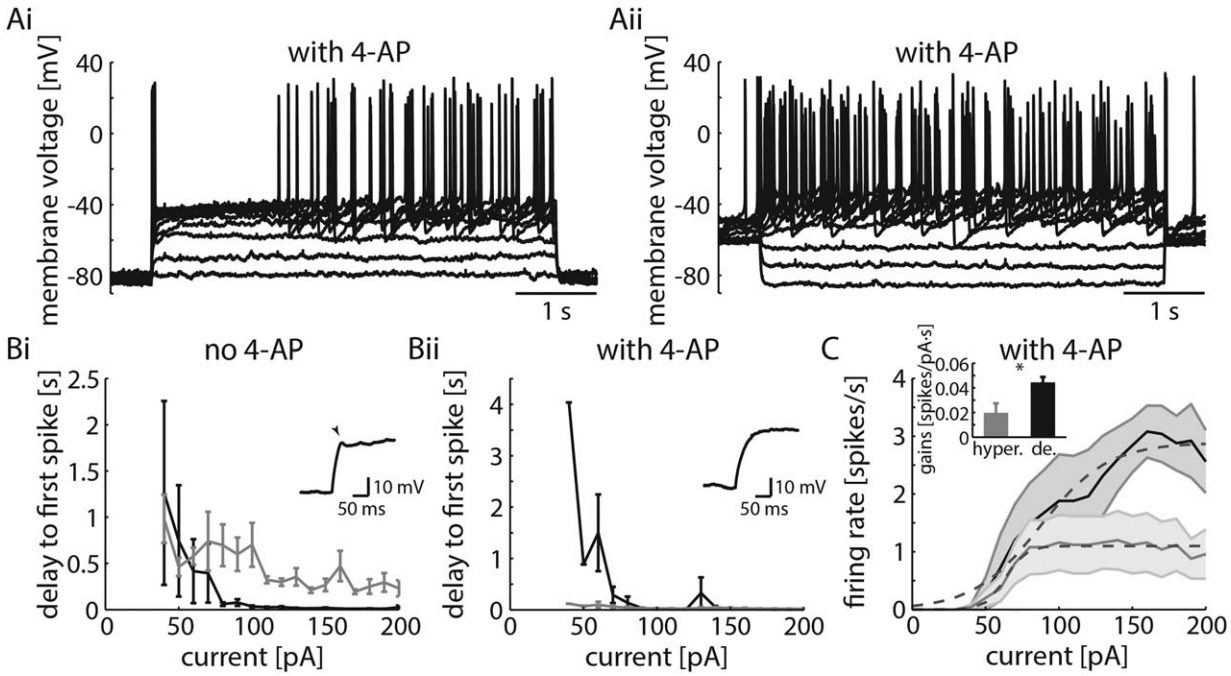

FIGURE 4. 4-AP-sensitive currents were not responsible for the divisive change in the *f-I* curve. A: Example traces of a cholinergic neuron with bath applied 10 mM 4-AP following hyperpolarization (*i*) and depolarization (*ii*). B: The presence of a delay to first spike following hyperpolarization (*i*), as well as the distinctive notch (arrowhead) and non-exponential charging curve (*i*, *inset*), resulted from the presence of an A-current in cholinergic MS-DB neurons without 4-AP. The delay (*ii*), non-exponential charging curve, and notch (*ii*, *inset*) were successfully eliminated following application of 4-AP. C: Average *f-I* curves with 4-AP indicated that the A-current was not responsible for the reduction in gain following hyperpolarization. Sigmoidal fits of average *f-I* curves (dashed lines) are for visualization purposes only.

During the range of steps, we measured a tail current that reversed at -93.1 ± 6.3 mV, which is consistent with a K^+ current ($n = 11$). Further, the maximum conductance was 34.1 ± 9.3 nS, indicating a relatively large K^+ conductance with the potential to significantly influence excitability (Fig. 5Ci; $n = 5$). The conductance began inactivating around -70 mV and was >80% inactivated around -40 mV, leaving a window conductance of 1.8 ± 0.7 nS at -44.3 ± 0.9 mV (i.e. an overlap between activation and inactivation curves) (Fig. 5Cii; $n = 5$). Each activation and inactivation curve was fit with a sigmoid, from which the midpoint ($V_{1/2}$) and slope (k) were extracted. The $V_{1/2}$ of activation for the K^+ current was -22.5 ± 1.3 mV, and the k was 8.1 ± 3.6 mV (Fig. 5Cii; $n = 5$), while the $V_{1/2}$ of inactivation was -60.2 ± 1.0 mV, and the k was -5.7 ± 1.1 mV (Fig. 5Cii; $n = 5$). The time constants of activation and inactivation were 152.7 ± 19.2 ms (a range of 9.3 ms to 575.1 ms) and 11.1 ± 1.6 s (a range of 3.3 s to 55.4 s), respectively ($n = 5$ for activation and 4 for inactivation). Our attempts to find a specific blocker of the current with various drugs, including the K^+ channel blockers 4-AP (10 mM), Hongotoxin-1 (10 nM), and XE991 (20 μM), were not successful. We did, however, discover that blocking the current was possible with 20 mM TEA. Because TEA simultaneously blocked K^+ channels crucial for normal action potential repolarization, we could not ascertain the involvement of the slow K^+ current in reducing firing rate and gain using a pharmacological approach.

As indicated, activation of the K^+ conductance occurred in the suprathreshold voltage region. To confirm this in current-clamp, we measured the subthreshold *I-V* curves following hyperpolarization and depolarization. From this, we derived the subthreshold membrane input resistance curves by taking the slopes of a running linear fit of the *I-V* curves (see Methods). The *I-V* curves showed little difference following hyperpolarization and depolarization (Fig. 5Di; $P = 0.0425$, two-way ANOVA; $n = 35$ neurons), with no significant difference in membrane input resistance across the entire subthreshold voltage region (Fig. 5Dii; $P = 0.7168$, two-way ANOVA; $n = 35$ neurons). These results confirm that any differences that could lead to changes in firing rate or gain are the result of the K^+ conductance activation in the suprathreshold voltage region.

Reduced Firing Rate and Gain Is Associated with Minimal Changes in Spike Shape

Next, we sought to understand how the slowly inactivating K^+ current reduced firing rate and gain. The change in firing rate and current threshold is easily explained by the hyperpolarizing current associated with recruiting K^+ currents at or near spike threshold. The reduction in gain, however, is more difficult to explain due to the slow kinetics of the K^+ current we observed in voltage-clamp. Often, reducing the gain of a neuron requires a current that activates within the time-frame of a spike and is able to significantly influence spike parameters,

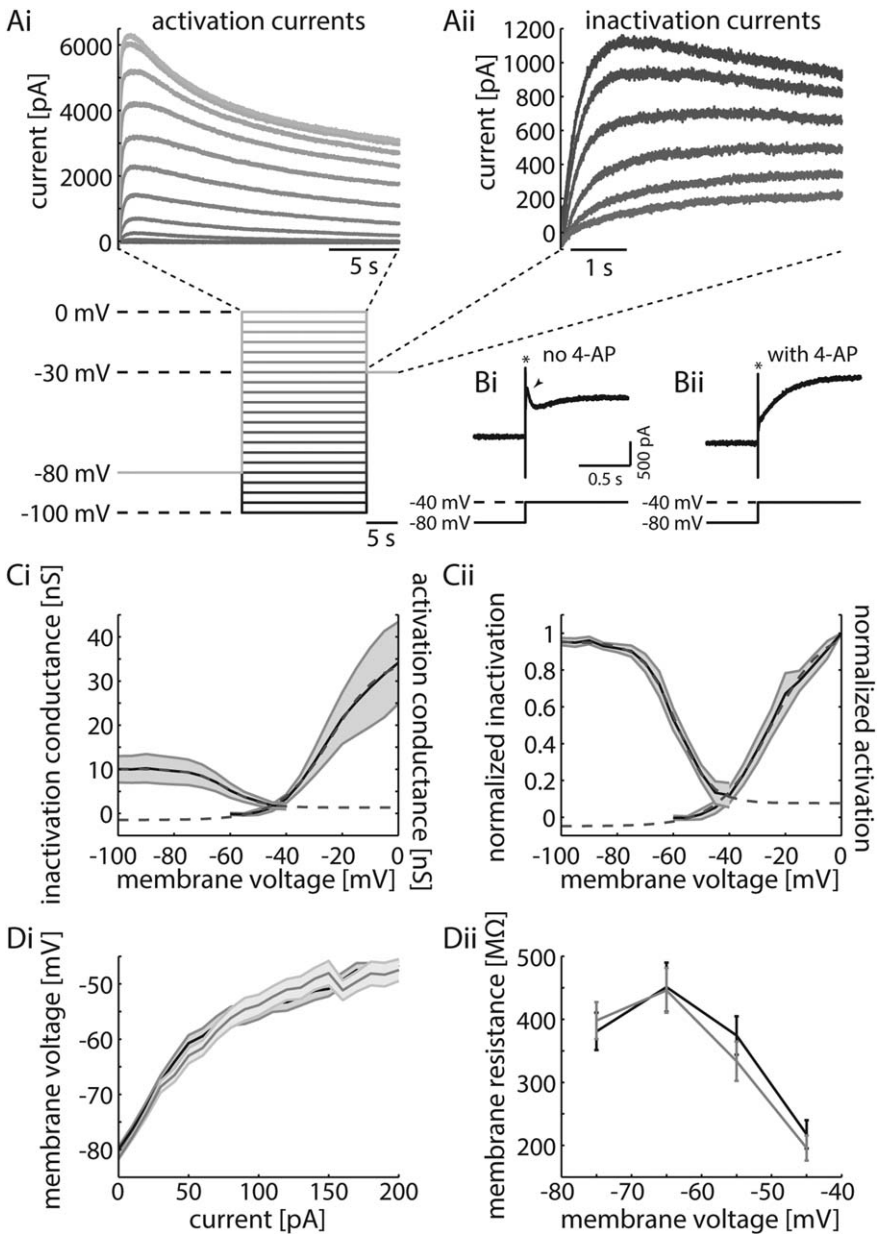

FIGURE 5. Voltage-clamp measures revealed the presence of a slow inactivating, outward current. A: Following hyperpolarization to −80 mV, voltage was stepped to values ranging from −100 mV to 0 mV, and then to −30 mV (*bottom*). Current trace examples during the range of voltage steps (*i*) showed the activation characteristics of the outward, slowly inactivating current, whereas current trace examples during the final step to −30 mV (*ii*) showed the inactivation characteristics. B: Representative trace showing the A-current (*i*; arrowhead points to A-current), which largely inactivated prior to the peak of the slower outward current. Addition of 4-AP eliminated the presence of the A-current (*ii*). Asterisks indicate capacitive transients. C: The maximum conductance values in response to depolarizing voltage steps were used to calculate the activation curve, while the maximum conductance values in response to a step to −30 mV were used to measure the inactivation curve (*i*, dashed lines). Conductances were calculated using $g = I/(V - E)$ and an experimentally derived reversal potential (E) of −93.1 mV. The normalized activation and inactivation curves are also shown (*ii*, dashed lines; $V_{1/2a} = -22.5 \pm 1.3$ mV, $k_a = 8.1 \pm 3.6$ mV; $V_{1/2i} = -60.2 \pm 1.0$ mV, $k_i = -5.7 \pm 1.1$ mV). D: Following hyperpolarization (gray) and depolarization (black), subthreshold *I-V* curves (*i*) were only slightly different, and resistance curves (*ii*) were not significantly different, indicating that the pertinent current activated in the suprathreshold voltage range.

such as the AHP depth and duration. Recruitment of the K^+ current following hyperpolarization should change spike parameters so as to decrease membrane excitability. For example, a cumulative loss of Na^+ current or an increase of K^+ current can lead to a divisive change in the *f-I* curve by altering the spike rate of rise or the AHP depth and duration, respectively (Fleidervish et al., 1996; Melnick et al., 2004; Mehaffey, 2005; Higgs et al., 2006; Fernandez and White, 2010).

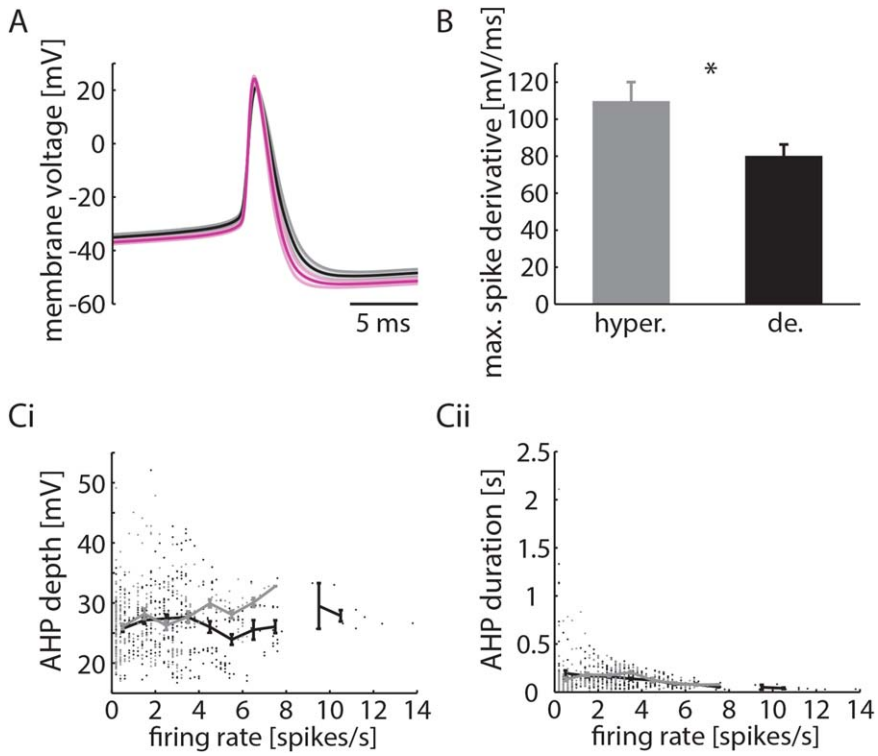

FIGURE 6. Characterization of spike shape following hyperpolarization. A: Average spike shape following hyperpolarization (purple) and depolarization (black). B: Average maximum derivative of the spikes used for A. Spikes following hyperpolarization had a significantly faster rise time, consistent with greater Na^+ conductance availability during the rising phase of the spike. C: AHP depth (*i*) following hyperpolarization (gray) was unaffected for low frequencies (0.2 − 4 Hz), although significantly deeper AHPs were seen at higher frequencies (4.2 − 7 Hz) than those seen following depolarization (black). AHP duration (*ii*) did not change following hyperpolarization. [Color figure can be viewed at wileyonlinelibrary.com]

To make these measures and test if recruitment of the K^+ current following hyperpolarization could alter spike shape, we took the average membrane voltage of spikes following hyperpolarization and compared it to the average spike generated following depolarization. To maximize the potential for observing differences in spike shape, we took the average spike waveform from the last spike of the current step that generated the highest mean firing rate (4.4 ± 0.5 spikes/s); higher firing rates have been established to generate greater spike frequency adaptation and alterations in spike waveform (Fleidervish et al., 1996; Fernandez and White, 2010). Thus, if there were four spikes following hyperpolarization, then the fourth spike was also selected from the corresponding current step following depolarization (Fig. 6A; $n = 24$ neurons).

To start, we measured the rate of rise, a surrogate for Na^+ current availability. Although an unlikely candidate for the observed decrease in gain, we nevertheless measured Na^+ current availability to eliminate the possible explanation of Na^+ current loss through a more complex interaction with K^+ currents and membrane voltage. Furthermore, past work has shown that a loss of Na^+ current can significantly impact gain (Fernandez and White, 2010). As indicated by the maximum derivative of the spike, we observed a steeper rate of rise in the spike waveform, and hence greater availability of Na^+ current, following hyperpolarizing pulses, a result inconsistent with reduced membrane excitability, firing rate, and gain (109.5 ± 10.5 mV/ms following hyperpolarization vs. 79.9 ± 6.4 mV/ms following depolarization; Fig. 6B; $P < 0.001$, two-tailed paired *t*-test; $n = 24$ neurons). Instead, our results are consistent with conventional explanations for increases in firing rate following hyperpolarization: hyperpolarization deinactivates Na^+ channels, allowing greater activation of those channels during subsequent depolarizing inputs. Thus, despite an increase in Na^+ current availability, hyperpolarization still led to a substantial decrease in the excitability of cholinergic neurons. An increase in the depth and duration of the AHP could indicate an increase in K^+ current availability that could account for the reduction in gain (Mehaffey, 2005; Higgs et al., 2006) following hyperpolarization. We characterized the AHP by measuring its depth and duration (see Methods) at various frequencies (1 spike/s sized frequency bins). We observed a slight, non-significant increase in AHP depth following hyperpolarization (Fig. 6Ci; $P = 0.0799$, two-way ANOVA; $n = 35$ neurons). The AHPs at higher frequencies (4.2 to 7 spikes/s) had a significantly different average depth (29.1 ± 0.4 mV following hyperpolarization vs. 24.9 ± 0.6 mV following depolarization; $0.0006 \leq P \leq 0.0495$; two-tailed unpaired *t*-tests for each frequency bin; $n = 3$ to 10 neurons).

This is in contrast to firing rates at or below 4 spikes/s, in which AHP depths were not significantly different (26.8 ± 0.2 mV following hyperpolarization vs. 27.0 ± 0.2 mV following depolarization; $0.3 \leq P \leq 0.6$; two-tailed unpaired *t*-tests for each frequency bin; $n = 8$ to 35 neurons). AHP durations also remained unchanged between the two conditions, with average durations of 151.3 ± 6.0 ms following hyperpolarization and 148.8 ± 5.0 ms following depolarization (Fig. 6Cii; $P = 0.6773$, two-way ANOVA; $n = 35$ neurons).

In summary, although we observed an increase in AHP depth at higher frequencies following hyperpolarization, changes to spike shape were very modest relative to the changes in firing rate and gain. In particular, compared to previous studies linking spike shape and gain (Kernell, 1965; Baldissera and Gustafsson, 1974; Madison and Nicoll, 1984), the changes we observed in cholinergic neurons were small and seem unlikely to influence gain. This is consistent with the slow kinetics of the K^+ current, which significantly limit recruitment within the time frame of an individual spike.

The Introduction of a Slowly Inactivating, Outward K^+ Current Allows for a Subtractive, but not Divisive, Change in the *f-I* Curve of a Model Neuron with a Steep *f-V* Curve

Although the recruitment of the K^+ current did not significantly influence spike shape, we speculated that it could significantly alter gain through another mechanism. To further explore the issue, we used the voltage-clamp data of the K^+ current in conjunction with a spike generating model to probe how or if a slow K^+ current could be recruited during spiking and influence threshold and gain.

For our model, we chose the exponential leaky integrate-and-fire (eLIF) model; this model is effective at reproducing a wide range of electrophysiological behaviors with a relatively small number of parameters (Fourcaud-Trocmé et al., 2003; Brette and Gerstner, 2005; Clopath et al., 2007; Naud et al., 2008; Fernandez et al., 2015). Critically, unlike the standard leaky integrate-and-fire (LIF) model, this model incorporates a real spike threshold. For the passive membrane properties used in the eLIF, we used values for input resistance and capacitance from the range of values we observed experimentally ($R = 118$-760 MΩ; $C = 39$-163 pF). Where possible, all model parameters matched the mean measured values from our experiments (see Methods). In accordance with previous studies that have used the eLIF model, we chose a value of $\Delta_T = 2$ mV (Δ_T: 1-6 mV, Fourcaud-Trocmé et al., 2003; 2 mV, Brette and Gerstner, 2005; 3.48 mV, Geisler et al., 2005; 0.8-5.5 mV, Naud et al., 2008; 2 mV, Touboul and Brette, 2008; 3.4-6.5 mV, Platkiewicz and Brette, 2010; 3 mV, Steimer and Schindler, 2015). Finally, we introduced the slowly inactivating K^+ current (I_{siK}) observed in our voltage-clamp data, with a reversal of -93.1 mV and a maximum conductance of 30.1 nS. Noise was also added to the model (SD = 0.6 ± 0.0006 mV) to mimic the relatively large intrinsic membrane voltage fluctuations present in these neurons in the presence of synaptic blockers (SD = 0.6 ± 0.1 mV at -81.5 ± 0.2 mV) (White et al., 2000).

To measure the *f-I* curve in the model neuron, we delivered a 200 pA range of current in 5 pA steps, with steps following either hyperpolarization (-79.5 ± 0.0009 mV) or depolarization (-58.0 ± 0.0006 mV), similar to our *in vitro* experimental protocol.

As shown, hyperpolarization has a largely subtractive effect on the *f-I* curve, with a gain of 734.0 ± 0.9 spikes/nA·s following hyperpolarization and 557.5 ± 16.3 spikes/nA·s following depolarization that results in a change in normalized gain $\left(\frac{\text{hyperpolarized}}{\text{depolarized}}\right)$ of 1.3 ± 0.04 (Fig. 7B, inset; $n = 50$ simulations). In this case, the lower gain following depolarization is due to the influence of small amounts of noise-induced spikes at low currents on the average *f-I* and *f-V* curve slopes; the current step-induced spiking increased with a slope very similar to hyperpolarized simulations. To better understand why hyperpolarization did not reduce the gain of the *f-I* curve, we plotted the relationship between firing rate and I_{siK}. Although hyperpolarization leads to an initial increase in I_{siK} relative to the depolarized condition, the difference in I_{siK} recruitment remains constant with increasing firing rates (Fig. 7C). Because of the voltage-dependent nature of I_{siK}, we next plotted the *f-V* curve to see if increasing firing rate in the model is associated with depolarization. The model expresses a steep *f-V* curve, with a gain of 84.8 ± 3.8 spikes/mV·s following hyperpolarization and 22.4 ± 4.6 spikes/mV·s following depolarization. Thus membrane voltage is effectively clamped to a near-threshold voltage that precludes significant activation of I_{siK} (Fig. 7D). In other words, the small range of voltages (0.6 ± 0.03 mV; from -58.2 ± 0.03 mV to -57.6 ± 0.004 mV for pulses following hyperpolarization) over which spikes are generated prevents increases in firing rate from recruiting greater amounts of I_{siK}. For this reason, hyperpolarization leads to a translation of the frequency vs. I_{siK} activation curve. On the other hand, a divisive effect on the *f-I* curve would be associated with a frequency-dependent recruitment of the current, with increasing depolarization generating greater activation of I_{siK}.

Cholinergic MS-DB Neurons Have Shallow *f-V* Curves

Our modeling results suggest that a steep *f-V* curve prevents a slowly activating and voltage-dependent K^+ current from increasing its activation level with increasing firing rate. However, the nature of the *f-V* curve in cholinergic MS-DB neurons in unknown. Our previous work in medial entorhinal cortical stellate neurons has shown that neurons can express shallow *f-V* curves that significantly depart from those expressed in established models of spike discharge (Fernandez et al., 2015).

We measured the *f-V* curves by averaging the membrane potential during each current pulse used for the *f-I* curves. We also measured the firing rate using the same methods as the *f-I* curves. In contrast to our model, we found an extremely shallow *f-V* curve that overlapped substantially with the slow K^+ conductance activation curve. Similar to the experimental *f-I* curves, trials where current pulses followed hyperpolarization

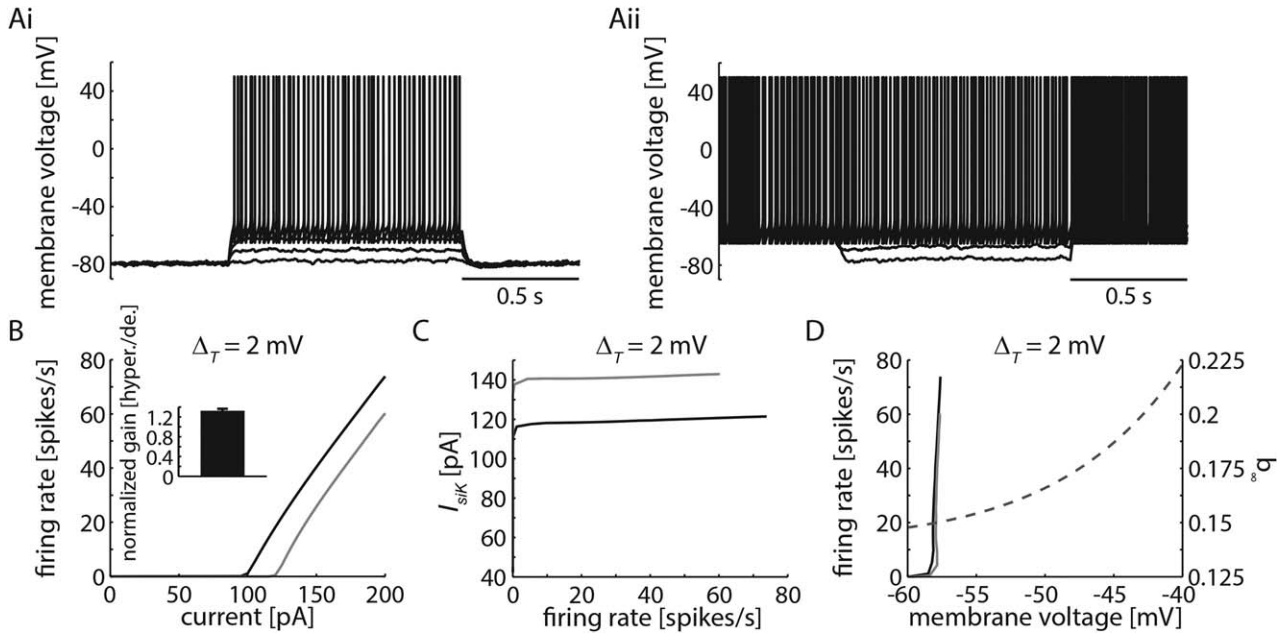

FIGURE 7. eLIF model ($\Delta_T = 2$ mV) with a slowly inactivating K^+ current (I_{siK}) and steep *f-V* curve shows a subtractive change in the *f-I* curve. A: Example traces from the model show similar spiking characteristics following hyperpolarization (*i*) and depolarization (*ii*). B: Model shows a subtractive, rather than divisive, *f-I* curve change following hyperpolarization. C: I_{siK} levels are steady across a range of firing rates, and the difference in current following hyperpolarization and depolarization remains constant. D: Model *f-V* curves are similar following hyperpolarization and depolarization; both are steep and effectively clamp voltage to a narrow range, despite the wide range of firing rates, preventing an increase in I_{siK} activation (dashed line).

resulted in a shallower *f-V* curve than those following depolarization. The gains in these instances were significantly different at 0.1 ± 0.1 spikes/mV·s following hyperpolarization and 0.2 ± 0.1 spikes/mV·s following depolarization (Fig. 8B, inset; $P = 0.042$, two-tailed paired *t*-test; $n = 31$ neurons).

Firing occurred over a wide range of 6.5 ± 0.8 mV (-48.5 ± 1.0 mV to -43.7 ± 0.8 mV; Fig. 8B; $n = 23$ neurons) following hyperpolarization and 7.6 ± 1.1 mV (-47.0 ± 0.9 mV to -40.3 ± 1.1 mV; Fig. 8B; $n = 29$ neurons) following depolarization. Similarly, the average suprathreshold interspike voltage had a range of 6.8 ± 0.8 mV (-47.2 ± 0.8 mV to -40.3 ± 0.7 mV) following hyperpolarization and 9.0 ± 1.2 mV (-45.6 ± 0.7 mV to -36.5 ± 1.1 mV) following depolarization, confirming the large changes in voltage with increases in injected current and firing rate (Fig. 8C). The shallow *f-V* curve in cholinergic MS-DB neurons is in contrast to the steep *f-V* curve of our model neuron and, in agreement with the results from Patel and Burdakov (2015), provides a means whereby the slowly inactivating and voltage-dependent K^+ current can increase its activation as a function of spike firing rate.

Gain Changes through the Introduction of a Slowly Inactivating K^+ Current Require Shallow *f-V* Curves in an eLIF Model

We hypothesized that the voltage-dependent nature of the slowly inactivating K^+ current, combined with the shallow *f-V* curves we observed in cholinergic MS-DB neurons, allow for the current to be recruited in a spike frequency-dependent manner and decrease the *f-I* curve gain. In order to confirm our hypothesis, we changed our model to include a shallow *f-V* curve. Because our previous work has shown that the Δ_T variable in the eLIF model has a drastic effect on the slope of the *f-V* curve (Fernandez et al., 2015), we chose a larger $\Delta_T = 10$ mV in order to obtain a shallower *f-V* curve.

We found that increasing Δ_T to 10 mV results in a 0.5 ± 0.02-fold reduction in gain, with gains of 79.0 ± 2.7 spikes/nA·s following hyperpolarization (-79.1 ± 0.001 mV) and 170.3 ± 7.0 spikes/nA·s following depolarization (-46.9 ± 0.001 mV), and hence similar to the 0.5-fold change seen in our experiments (Fig. 9B, inset; $n = 50$ simulations). The reduction in gain holds true for a range of $V_{1/2}$ values (normalized gains of 0.81 ± 0.04 to 0.08 ± 0.003 following hyperpolarization for {$V_{1/2}$ activation, $V_{1/2}$ inactivation} = {-21.46, −59.23} mV to {-32.46, −70.23} mV, respectively) and *k* values (normalized gains of 0.92 ± 0.04 to 0.16 ± 0.01 following hyperpolarization for {*k* activation, *k* inactivation} = {13.08, −0.69} mV to {6.08, −7.69} mV, respectively), indicating that a reduction in gain could be attained with a range of parameters. In contrast to our results with $\Delta_T = 2$ mV, I_{siK} activation increases with increasing spike firing rate once $\Delta_T = 10$ mV and the *f-V* curve is shallow. Following hyperpolarization, more I_{siK} was recruited per spike, as well as on average at maximum firing rates compared to values following depolarization (Fig. 9C). The *f-V* curve of the model with $\Delta_T = 10$ mV is shallow, with a gain of 0.4 ± 0.02 spikes/mV·s following hyperpolarization and 3.0 ± 0.3 spikes/

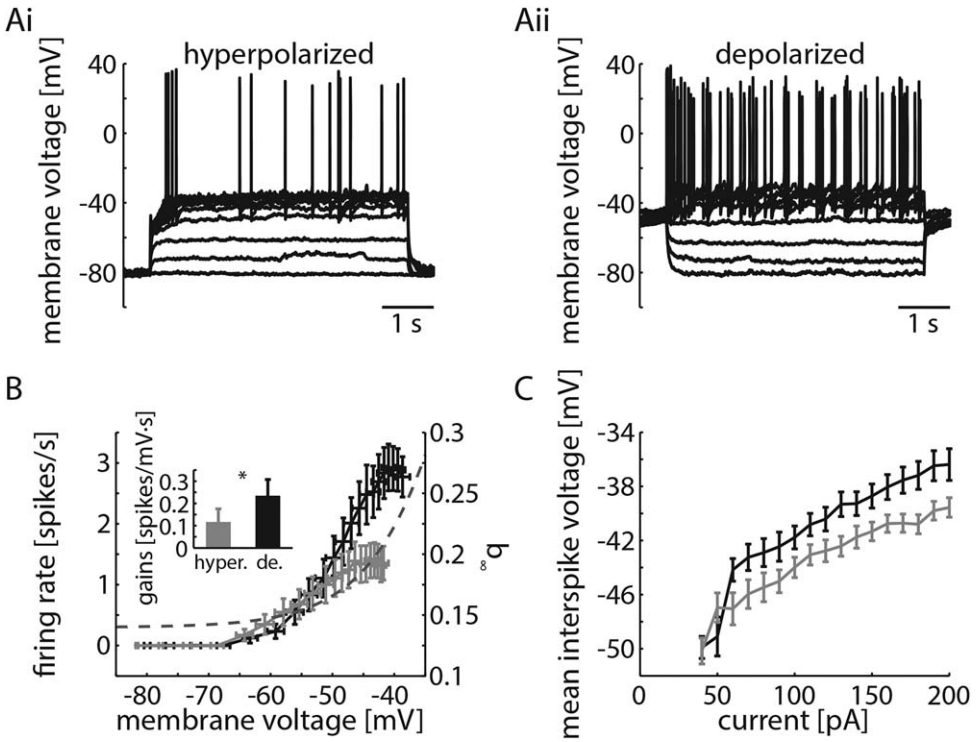

FIGURE 8. Cholinergic neurons in the MS-DB had shallow *f-V* curves. A: Example voltage traces from a cholinergic MS-DB neuron following hyperpolarization (*i*) and depolarization (*ii*). B: These neurons had shallow *f-V* curves which overlapped with the slow K^+ current activation (dashed line) to a greater degree than the model and were divisively changed following hyperpolarization. C: Suprathreshold *I-V* curves following hyperpolarization and depolarization spanned a wide range of voltages, which is consistent with the shallow *f-V* curves.

mV·s following depolarization; spiking occurred over a wide range of voltages (5.1 ± 0.1 mV; from -49.3 ± 0.1 mV to -44.2 ± 0.1 mV for pulses following hyperpolarization), with more overlap with the range of voltages over which the slow K^+ current activated (Fig. 9D).

A shallow *f-V* curve is a critical feature for *f-I* gain changes in our model. Consistent with the results from Patel and Burdakov (2015), we have shown with our modeling and experimental work that gain changes by I_{siK} are possible when the voltage window (the voltage range shown in the *f-V* and suprathreshold *I-V* curves in Figs. 8B and 8C, respectively) overlaps with the activation curve of the current (Fig. 5Cii). This is more likely with a wide voltage window, or when the *f-V* curve is shallow. Thus, our model shows that divisive changes to the *f-I* curve are possible with introduction of a slowly inactivating, outward K^+ current, provided the neuron also has an *f-V* curve with a shallow profile. Hyperpolarization acts to allow recruitment of the K^+ current, reducing both the firing rate and gain.

DISCUSSION

We present evidence of changes in the input-output properties of cholinergic MS-DB neurons in response to hyperpolarizing inputs. These changes, which include reductions in firing rate and gain, are specific to cholinergic neurons. Further, we measured and characterized a slowly inactivating K^+ current and an experimentally verified shallow *f-V* curve, which together can account for the reduction in gain following hyperpolarization.

Implications for Cholinergic MS-DB Neuron Control of Hippocampal Theta Oscillations

Cholinergic MS-DB neurons receive local input from GABAergic and glutamatergic neurons, as well as excitatory input from the hypothalamus and inhibitory feedback from hippocamposeptal neurons (Gerashchenko et al., 2001; Colom et al., 2005; Leão et al., 2015). Since their relay of depolarizing inputs to hippocampal pyramidal and basket neurons may control the amplitude of hippocampal theta, modulation of cholinergic MS-DB neuron gain may change the hippocampal oscillatory state.

Our present work suggests that hyperpolarization acts as a switch by which cholinergic MS-DB neuron spike firing rate and gain is controlled. When cholinergic MS-DB neuron gain is high (without hyperpolarization), their responsiveness to synaptic input is high, which likely increases the amount of acetylcholine delivered to hippocampal neurons. Cholinergic input

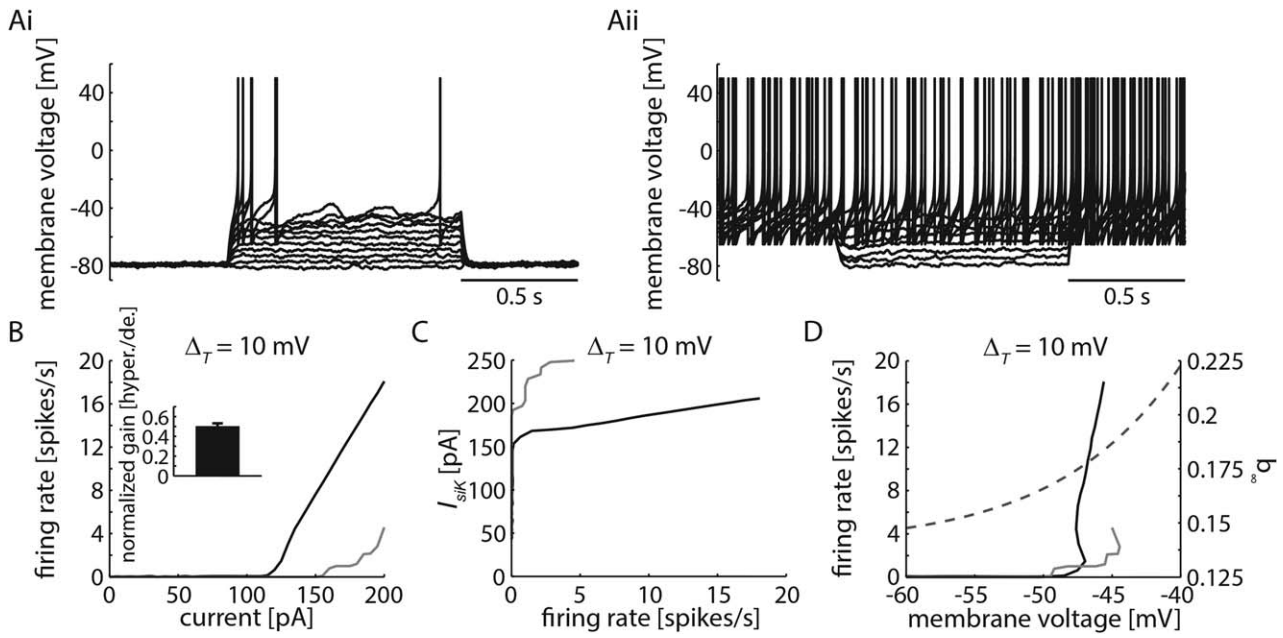

FIGURE 9. eLIF model ($\Delta_T = 10$ mV) with I_{siK} and a shallow *f-V* curve shows a divisive change in the *f-I* curve. A: Example traces from the model show much lower firing rates following hyperpolarization (*i*) than those following depolarization (*ii*). B: Model shows a divisive *f-I* curve change, with a normalized change in gain that is similar to experimental results (*inset*), following hyperpolarization. C: I_{siK} levels change across a range of firing rates, with steeper increases and higher maximum current values evoked following hyperpolarization. D: Model *f-V* curves with $\Delta_T = 10$ mV are shallow following hyperpolarization, covering a range of voltages that increases I_{siK} activation (dashed line) as firing rate increases.

to the hippocampus is responsible for long-lasting depolarization of hippocampal neurons (Dodd et al., 1981; Cole and Nicoll, 1983, 1984), possibly promoting theta. On the other hand, when cholinergic MS-DB neuron gain is low (following hyperpolarization), their responsiveness to synaptic input will also be low, decreasing the amount of acetylcholine released on hippocampal neurons, and thus decreasing theta amplitude. In addition, cholinergic MS-DB neurons may also be indirectly involved in hippocampal theta via their local connections to GABAergic and glutamatergic neurons.

Implications for Cholinergic MS-DB Neuron Control of Hippocampal SPW-Rs

Previous work has shown that MS-DB neuronal activity is suppressed during SPW-R events (Dragoi et al., 1999). Mattis et al. (2014) reported that optogenetic stimulation of hippocamposeptal inhibitory neurons at SPW-R frequencies (50 Hz) was more effective at driving long-lasting hyperpolarization of cholinergic MS-DB neurons than theta frequency stimulation (8 Hz). When taken together with our results, this suggests that SPW-R frequencies in the hippocampus actively suppress theta rhythms though hyperpolarization of cholinergic MS-DB neurons. This hyperpolarization, in turn, may lower the gain of cholinergic MS-DB neurons and decrease their contribution to the hippocampal theta rhythm. On the other hand, when hippocamposeptal neurons (which reflect hippocampal pyramidal neuron firing rates) fire at theta frequencies, cholinergic MS-DB neurons are not as hyperpolarized, their gain is not suppressed, and they can respond with greater sensitivity to local and non-local inputs.

One caveat to this hypothesis is that single SPW-R events are of shorter duration than the SPW-R frequency stimulation of hippocamposeptal neurons performed in Mattis et al. (2014), and thus may not lead to large hyperpolarization of cholinergic neurons. However, it is possible that shorter duration SPW-R frequency hippocamposeptal neuron activity still has significant effects on cholinergic neuron membrane voltage and gain. Also consistent with this hypothesis, a recent study has shown that optogenetic activation of cholinergic MS-DB neurons blocked SPW-Rs in the hippocampus, while increasing theta power and coherence (Vandecasteele et al., 2014). It is therefore possible that hippocamposeptal neurons *dis*inhibit SPW-Rs by suppressing cholinergic MS-DB neuronal activity.

The degree of hyperpolarization presented in Figure 1 is larger than that seen in Mattis et al. (2014), and thus the resulting effect may be larger than under more physiological conditions. Our analysis of the levels of hyperpolarization necessary to evoke the effect, however, suggests that the reduction in firing rate comes on gradually as hyperpolarization increases, such that even small levels of hyperpolarization result in some level of firing rate reduction. In addition, membrane potential in other types of neurons in awake and anesthetized mice is dominated by large (SD $>$ 2 mV), low frequency ($f <$ 5 Hz)

fluctuations (Paré et al., 1998; Destexhe et al., 2003; Crochet and Petersen, 2006; Constantinople and Bruno, 2011; Sachidhanandam et al., 2013). If present in cholinergic MS-DB neurons *in vivo*, low frequency membrane potential fluctuations could elicit robust changes in gain. Moreover, the gain reduction persisted in the presence of artificially-generated membrane voltage fluctuations mimicking *in vivo* conditions. It would be possible to test the effects of hippocamposeptal-induced hyperpolarization by testing the gain of cholinergic MS-DB neurons following optogenetic stimulation of hippocamposeptal axons or neurons.

Future *in vivo* experiments that test the role of hyperpolarization-induced gain reduction in the disinhibition of SPW-Rs will be needed. If our hypothesis is correct, selective block of the slowly inactivating K^+ current present in cholinergic MS-DB neurons may lead to learning deficits due to impaired SPW-Rs and memory consolidation. In addition, Mattis et al. (2014) reported that long-lasting hippocamposeptal hyperpolarization of cholinergic neurons was sensitive to GIRK channel and D_2 dopamine receptor antagonists. This G-protein-coupled response is in contrast to the GABAergic response evoked by theta frequency stimulation of hippocamposeptal neurons. Therefore, it may be possible to observe reductions in the firing rate and gain of these neurons, and perhaps increases in hippocampal SPW-Rs, through local application of GIRK channel and D_2 receptor agonists.

Voltage-Dependent Gain Modulation in Cholinergic MS-DB Neurons

Our voltage-clamp measures indicate the presence of a slowly activating and inactivating K^+ current that activates at suprathreshold voltage values. In combination with the shallow *f-V* curve, the increased activation of the K^+ current leads to a divisive effect on the *f-I* curve of cholinergic neurons. The divisive change occurs when depolarization increases with firing rate (shallow *f-V* curve), which enables the K^+ current to increase its average conductance at higher spike firing rates.

Generally, models of spike discharge express a flat *I-V* curve, along with a correspondingly steep *f-V* curve (Holt and Koch, 1997; Mitchell and Silver, 2003; Prescott and De Koninck, 2003). In fact, a flat *I-V* curve is a feature that has been used to account for the numerous effects of synaptic input and shunting conductance on input-output modulation in neurons (Holt and Koch, 1997; Doiron et al., 2001; Ulrich, 2003). In particular, Holt and Koch (1997) describe an LIF model in which the spiking mechanism clamps membrane voltage to approximately −50 mV. Because the voltage trajectory between spikes in the LIF model is exponential, with a relatively short membrane time constant, membrane voltage largely hovers near the asymptotic value. This, along with the spike reset mechanism, effectively clamps membrane voltage during spiking somewhere between the reset value and the asymptotic value of the exponential trajectory. Further, increasing the spike firing rate does little to change the mean voltage trajectory since the mean of an individual exponential trajectory between spikes changes little with higher input currents.

Positively sloped and shallow *f-V* curves, however, may be a common characteristic of biological neurons (Fernandez et al., 2011, 2015; our present work). In part, this is because the evolution of the membrane voltage trajectory between spikes is rarely exponential, as it is influenced by numerous voltage-gated conductances that activate, deactivate or inactivate during and after the spike refractory period. As a result, in biological neurons, the mean value of the voltage trajectory during spiking can depolarize with increasing firing rate and input current. This is in sharp contrast to the linear behavior in the LIF that can only generate an exponential trajectory, whereby the firing rate has little impact on the mean voltage value during spiking.

It is common for studies using the eLIF model to use small Δ_T values, as it accurately reproduces the spike onset behavior observed in biological neurons. Under these conditions, however, the *f-V* curve remains similar to the LIF model. This is because the evolution of the membrane voltage trajectory is largely exponential and is only influenced by the Δ_T parameter in the immediate vicinity of spike threshold. The shallow *f-V* curve we measured in cholinergic MS-DB neurons led us to choose a Δ_T value of 10 mV that generates a shallow *f-V* curve in accordance to mechanisms described by Fernandez et al. (2015). Although $\Delta_T = 10$ mV is higher than Δ_T values derived from analysis of neuronal Na^+ channel activation kinetics (Angelino and Brenner, 2007), it provides a simple method by which to reproduce a fundamental feature of neuronal *f-V* curves. The origin of shallow *f-V* curves is complex and likely originates from a multitude of factors that differ between neuron types, and are beyond the scope of this paper. Fundamentally, the expression of a shallow *f-V* curve is critical, as neurons express voltage-gated conductances with similarly shallow activation curves. Thus, whether our simplified model accurately describes the biophysical origin of the shallow *f-V* curve is of secondary importance to the fact that it generates a more biologically accurate *f-V* relationship. Once present, the model with a shallow *f-V* curve easily scales its firing rate and gain in the presence of a slowly activating and inactivating K^+ conductance.

Identity of the Slowly Inactivating Outward Current

The simplest way to test the role of the slowly inactivating outward current in the input-output properties of cholinergic MS-DB neurons would be to use specific channel antagonists. By using a specific blocker of the current, we would be able to observe if hyperpolarizing inputs still cause subsequent reductions in firing rate and gain. Because of the −93.1 mV reversal potential, indicating a K^+ dominated current, and because of the slow activation and inactivation kinetics of the current, we selected blockers of Kv1, Kv7, and other K^+ channels. Although we attempted to block the current with 4-AP, XE991, hongotoxin-1, and TEA, none of the drugs completely and specifically blocked the current. TEA did block the current, but in

a non-specific way, making it impossible to ascertain the influence of the current on input-output properties. Future work will be needed to identify the constituent channels of the current, providing a means whereby their necessity in firing rate and gain reductions can be tested more directly.

REFERENCES

Alonso A, Köhler C. 1982. Evidence for separate projections of hippocampal pyramidal and non-pyramidal neurons to different parts of the septum in the rat brain. Neurosci Lett 31:209–214.

Anderson JS, Lampl I, Gillespie DC, Ferster D. 2000. The contribution of noise to contrast invariance of orientation tuning in cat visual cortex. Science 290:1968–1972.

Angelino E, Brenner MP. 2007. Excitability constraints on voltage-gated sodium channels. PLoS Comput Biol 3:1751–1760.

Baldissera F, Gustafsson B. 1974. Firing behaviour of a neurone model based on the afterhyperpolarization conductance time course and algebraical summation. Adaptation and steady state firing. Acta Physiol Scand 92:27–47.

Bekkers JM. 2000. Properties of voltage-gated potassium currents in nucleated patches from large layer 5 cortical pyramidal neurons of the rat. J Physiol 525:593–609.

Berry SD, Thompson RF. 1978. Prediction of learning rate from the hippocampal electroencephalogram. Science 200:1298–1300.

Brette R, Gerstner W. 2005. Adaptive exponential integrate-and-fire model as an effective description of neuronal activity. J Neurophysiol 94:3637–3642.

Buzsáki G. 2005. Theta rhythm of navigation: link between path integration and landmark navigation, episodic and semantic memory. Hippocampus 15:827–840.

Chapman CA, Lacaille J-C. 1999. Cholinergic induction of theta-frequency oscillations in hippocampal inhibitory interneurons and pacing of pyramidal cell firing. J Neurosci 19:8637–8645.

Clopath C, Jolivet R, Rauch A, Lüscher H-R, Gerstner W. 2007. Predicting neuronal activity with simple models of the threshold type: adaptive exponential integrate-and-fire model with two compartments. Neurocomputing 70:1668–1673.

Cole AE, Nicoll RA. 1983. Acetylcholine mediates a slow synaptic potential in hippocampal pyramidal cells. Science 221:1299–1301.

Cole AE, Nicoll RA. 1984. Characterization of a slow cholinergic post-synaptic potential recorded in vitro from rat hippocampal pyramidal cells. J Physiol 352:173–188.

Colom LV, Castaneda MT, Reyna T, Hernandez S, Garrido-Sanabria E. 2005. Characterization of medial septal glutamatergic neurons and their projection to the hippocampus. Synapse 58:151–164.

Connor JA, Stevens CF. 1971. Prediction of repetitive firing behaviour from voltage clamp data on an isolated neurone soma. J Physiol 213:31–53.

Constantinople CM, Bruno RM. 2011. Effects and mechanisms of wakefulness on local cortical networks. Neuron 69:1061–1068.

Crochet S, Petersen CCH. 2006. Correlating whisker behavior with membrane potential in barrel cortex of awake mice. Nat Neurosci 9:608–610.

Destexhe A, Rudolph M, Paré D. 2003. The high-conductance state of neocortical neurons in vivo. Nat Rev Neurosci 4:739–751.

Dodd J, Dingledine R, Kelly JS. 1981. The excitatory action of acetylcholine on hippocampal neurones of the guinea pig and rat maintained in vitro. Brain Res 207:109–127.

Doiron B, Longtin A, Berman N, Maler L. 2001. Subtractive and divisive inhibition: Effect of voltage-dependent inhibitory conductances and noise. Neural Comput 13:227–248.

Dragoi G, Carpi D, Recce M, Csicsvari J, Buzsáki G. 1999. Interactions between hippocampus and medial septum during sharp waves and theta oscillation in the behaving rat. J Neurosci 19:6191–6199.

Fernandez FR, Broicher T, Truong A, White JA. 2011. Membrane voltage fluctuations reduce spike frequency adaptation and preserve output gain in CA1 pyramidal neurons in a high-conductance state. J Neurosci 31:3880–3893.

Fernandez FR, Malerba P, White JA. 2015. Non-linear membrane properties in entorhinal cortical stellate cells reduce modulation of input-output responses by voltage fluctuations. PLoS Comput Biol 11:e1004188.

Fernandez FR, White JA. 2010. Gain control in CA1 pyramidal cells using changes in somatic conductance. J Neurosci 30:230–241.

Fleidervish IA, Friedman A, Gutnick MJ. 1996. Slow inactivation of Na^+ current and slow cumulative spike adaptation in mouse and guinea-pig neocortical neurones in slices. J Physiol 493:83–97.

Fourcaud-Trocmé N, Hansel D, Vreeswijk CV, Brunel N. 2003. How spike generation mechanisms determine the neuronal response to fluctuating inputs. J Neurosci 23:11628–11640.

Geisler C, Brunel N, Wang X-J. 2005. Contributions of intrinsic membrane dynamics to fast network oscillations with irregular neuronal discharges. J Neurophysiol 94:4344–4361.

Gerashchenko D, Salin-Pascual R, Shiromani PJ. 2001. Effects of hypocretin-saporin injections into the medial septum on sleep and hippocampal theta. Brain Res 913:106–115.

Girardeau G, Benchenane K, Wiener SI, Buzsáki G, Zugaro MB. 2009. Selective suppression of hippocampal ripples impairs spatial memory. Nat Neurosci 12:1222–1223.

Griffith WH, Sim JA. 1990. Comparison of 4-aminopyridine and tetrahydroaminoacridine on basal forebrain neurons. J Pharmacol Exp Ther 255:986–993.

Hasselmo ME. 2005. What is the function of hippocampal theta rhythm?–Linking behavioral data to phasic properties of field potential and unit recording data. Hippocampus 15:936–949.

Heath NC, Rizwan AP, Engbers JDT, Anderson D, Zamponi GW, Turner RW. 2014. The expression pattern of a Cav3-Kv4 complex differentially regulates spike output in cerebellar granule cells. J Neurosci 34:8800–8812.

Higgs MH, Slee SJ, Spain WJ. 2006. Diversity of gain modulation by noise in neocortical neurons: regulation by the slow afterhyperpolarization conductance. J Neurosci 26:8787–8799.

Holt GR, Koch C. 1997. Shunting inhibition does not have a divisive effect on firing rates. Neural Comput 9:1001–1013.

Jinno S, Klausberger T, Marton LF, Dalezios Y, Roberts JDB, Fuentealba P, Bushong EA, Henze D, Buzsáki G, Somogyi P. 2007. Neuronal diversity in GABAergic long-range projections from the hippocampus. J Neurosci 27:8790–8804.

Kernell D. 1965. The limits of firing frequency in cat lumbosacral motoneurones possessing different time course of afterhyperpolarization. Acta Physiol Scand 65:87–100.

Kramis R, Vanderwolf CH, Bland BH. 1975. Two types of hippocampal rhythmical slow activity in both the rabbit and the rat: Relations to behavior and effects of atropine, diethyl ether, urethane, and pentobarbital. Exp Neurol 49:58–85.

Leão RN, Targino ZH, Colom LV, Fisahn A. 2015. Interconnection and synchronization of neuronal populations in the mouse medial septum/diagonal band of Broca. J Neurophysiol 113:971–980.

Lee MG, Chrobak JJ, Sik A, Wiley RG, Buzsáki G. 1994. Hippocampal theta activity following selective lesion of the septal cholinergic system. Neuroscience 62:1033–1047.

Lin RJ, Bettencourt J, White JA, Christini DJ, Butera RJ. 2010. Real-time experiment interface for biological control applications. Conf Proc IEEE Eng Med Biol Soc 1:4160–4163.

Madison DV, Nicoll RA. 1984. Control of the repetitive discharge of rat CA1 pyramidal neurones in vitro. J Physiol 354:319–331.

Magariños-Ascone C, Núñez Á, Delgado-García JM. 1999. Different discharge properties of rat facial nucleus motoneurons. Neuroscience 94:879–886.

Markram H, Segal M. 1990. Electrophysiological characteristics of cholinergic and non-cholinergic neurons in the rat medial septum-diagonal band complex. Brain Res 513:171–174.

Mattis J, Brill J, Evans S, Lerner TN, Davidson TJ, Hyun M, Ramakrishnan C, Deisseroth K, Huguenard JR. 2014. Frequency-dependent, cell type-divergent signaling in the hippocamposeptal projection. J Neurosci 34:11769–11780.

Mehaffey WH. 2005. Deterministic multiplicative gain control with active dendrites. J Neurosci 25:9968–9977.

Melnick IV, Santos SFA, Safronov BV. 2004. Mechanism of spike frequency adaptation in substantia gelatinosa neurones of rat. J Physiol 559:383–395.

Mitchell SJ, Silver RA. 2003. Shunting inhibition modulates neuronal gain during synaptic excitation. Neuron 38:433–445.

Naud R, Marcille N, Clopath C, Gerstner W. 2008. Firing patterns in the adaptive exponential integrate-and-fire model. Biol Cybern 99: 335–347.

Paré D, Shink E, Gaudreau H, Destexhe A, Lang EJ. 1998. Impact of spontaneous synaptic activity on the resting properties of cat neocortical pyramidal neurons in vivo. J Neurophysiol 79:1450–1460.

Patel AX, Burdakov D. 2015. Mechanisms of gain control by voltage-gated channels in intrinsically-firing neurons. PLoS One 10: e0115431.

Platkiewicz J, Brette R. 2010. A threshold equation for action potential initiation. PLoS Comput Biol 6:e1000850.

Prescott SA, De Koninck Y. 2003. Gain control of firing rate by shunting inhibition: roles of synaptic noise and dendritic saturation. Proc Natl Acad Sci USA 100:2076–2081.

Sachidhanandam S, Sreenivasan V, Kyriakatos A, Kremer Y, Petersen CCH. 2013. Membrane potential correlates of sensory perception in mouse barrel cortex. Nat Neurosci 16:1671–1677.

Segal M, Barker JL. 1984. Rat hippocampal neurons in culture: potassium conductances. J Neurophysiol 51:1409–1433.

Sotty F, Danik M, Manseau F, Laplante F, Quirion R, Williams S. 2003. Distinct electrophysiological properties of glutamatergic, cholinergic and GABAergic rat septohippocampal neurons: Novel implications for hippocampal rhythmicity. J Physiol 551:927–943.

Steimer A, Schindler K. 2015. Random sampling with interspike-intervals of the exponential integrate and fire neuron: A computational interpretation of UP-states. PLoS One 10:e0132906.

Takács VT, Freund TF, Gulyás AI. 2008. Types and synaptic connections of hippocampal inhibitory neurons reciprocally connected with the medial septum. Eur J Neurosci 28:148–164.

Tóth K, Borhegyi Z, Freund TF. 1993. Postsynaptic targets of GABAergic hippocampal neurons in the medial septum-diagonal band of Broca complex. J Neurosci 13:3712–3724.

Touboul J, Brette R. 2008. Dynamics and bifurcations of the adaptive exponential integrate-and-fire model. Biol Cybern 99:319–334.

Ulrich D. 2003. Differential arithmetic of shunting inhibition for voltage and spike rate in neocortical pyramidal cells. Eur J Neurosci 18:2159–2165.

Vandecasteele M, Varga V, Berényi A, Papp E, Barthó P, Venance L, Freund TF, Buzsáki G. 2014. Optogenetic activation of septal cholinergic neurons suppresses sharp wave ripples and enhances theta oscillations in the hippocampus. Proc Natl Acad Sci USA 111:13535–13540.

White JA, Rubinstein JT, Kay AR. 2000. Channel noise in neurons. Trends Neurosci 23:131–137.

Winson J. 1978. Loss of hippocampal theta rhythm results in spatial memory deficit in the rat. Science 201:160–163.

Zhang H, Lin S-C, Nicolelis MAL. 2011. A distinctive subpopulation of medial septal slow-firing neurons promote hippocampal activation and theta oscillations. J Neurophysiol 106:2749–2763.

Zona C, Pirrone G, Avoli M, Dichter M. 1988. Delayed and fast transient potassium currents in rat neocortical neurons in cell culture. Neurosci Lett 94:285–290.